Parity Violation Experiment at Mainz

J. Van de Wiele and M. Morlet

Institut de Physique Nucléaire/IN2P3, F-91406 Orsay Cedex, France

and the A4 Collaboration[(a,b,c,d)†)]

Received ;
final version

Measurement of asymmetry in polarized electron-nucleon elastic scattering provides information on the weak charge and current distributions in the nucleon through the interference between photon and Z^0 exchange graphs. This asymmetry is due to the parity violation in the weak interaction. The expansion of weak form factors in term of flavor (u,d,s) form factors leads to information on quark structure of the nucleon, especially on the strangeness contribution to the vector form factors. The measurement of the parity violating asymmetry in elastic scattering of polarized electrons on protons at MAMI facility in Mainz is presented. At the MAMI current energy of 0.8543 GeV, the electrons scattered out a 10 cm liquid hydrogen target are detected between 31.4° and 42.4°. Under these kinematic conditions, the value of the transfer momentum Q^2, weighted by the elastic cross section in this angular range, is $Q^2 = 0.236 \pm 0.025$ $(\mathrm{GeV/c})^2$. This experiment measures the $G_E^s + 0.218 G_M^s$ combination of the electric and magnetic strange form factors (for the mean scattering angle). The detection is done using a calorimeter built of 511 Čerenkov crystals in the phase I of the experiment. The experimental set-up with its main characteristics are shown. The origin and magnitude of possible systematic and helicity correlated false asymmetries are discussed.

PACS: *.*
Key words: Parity Violation, electron-proton elastic scattering, Strangeness,

1 Introduction

Parity violation in the scattering of polarized electrons provides an observable which is sensitive to the vector matrix element $< p|\bar{\psi}_s \gamma_\mu \psi_s|p >$. As the weak interaction violates the discrete symmetry of parity, the scattering of polarized electrons on unpolarized protons produces an asymmetry in the cross section. In this contribution, we are interested by the elastic scattering of polarized electrons off unpolarized protons in the kinematics governed by the MAMI facility in Mainz. The transition amplitude $\mathcal{T}(p'e', ep)$ of ep elastic electro-weak scattering is the sum of the elec-

†) (a) P. Achenbach, K. Aulenbacher, S. Baunack, B. Fiedler, K. Grimm, T. Hammel, D. von. Harrach, E. Kabuß, R. Kothe, K. W. Krygier, A. Loepes Ginja, F. E. Maas, E. Schilling, G. Stephan, C. Weinrich, H. Schmieden, P. Barstch, M. Seidl. *Institut für Kernphysik, Universität Mainz, Becherweg 45, D-55099 Mainz* (b) J. Arvieux, B. Collin, S. Essabaa, R. Frascaria, M. Guidal, H. Guler, R. Kunne, D. Marchand, M. Morlet, S. Ong, L. Rosier, J. Van de Wiele. *Institut de Physique Nucléaire/IN2P3, F-91406 Orsay Cedex, France* (c) I. Altarev. *St. Petersburg, Institut for Nuclear Research, RAS, St Petersburg 183550, Russia* (d) S. Kowalski. *M.I.T. Laboratory for Nuclear Science, Cambridge*

tromagnetic amplitude $\mathcal{T}^{EM}(p'e', ep)$ due to the exchange of a virtual photon and of the neutral current amplitude $\mathcal{T}^{NC}(p'e', ep)$ due to the exchange of the Z^0. As the neutral current amplitude is small compared to the electromagnetic amplitude ($\approx 10^{-5}$), the measured asymmetry defined as $A = \frac{\sigma_+ - \sigma_-}{\sigma_+ + \sigma_-}$ is practically due to the interference of the electromagnetic and neutral currents. In this expression σ_+ is the cross section associated with incident electron with an helicity equal to 1/2 and σ_- is the cross section associated with incident electron with an helicity equal to $-1/2$. The proton asymmetry, A_s^p is the sum of the term A_0^p which is known from elastic scattering cross section measurement and of a term which contains explicitly the strange form factors:

$$A_0^p = -\frac{\mathcal{K}}{4\sigma_p}\left[\xi_V^p \sigma_p + \xi_V^n \left(\varepsilon G_E^{p,\gamma} G_E^{n,\gamma} + \tau G_M^{p,\gamma} G_M^{n,\gamma}\right) - \varepsilon'' G_M^{p,\gamma} G_A^{T=1} - \varepsilon'' G_M^{p,\gamma} G_A^{T=0}\right] \quad (1)$$

$$A_s^p = A_0^p - \frac{\mathcal{K}}{4\sigma_p}\left[\xi_V^{(0)} \left(\varepsilon G_E^{p,\gamma} G_E^{s} + \tau G_M^{p,\gamma} G_M^{s}\right) - \varepsilon'' \xi_A^s G_M^{p,\gamma} G_A^{s}\right] \quad (2)$$

where
$$\varepsilon = \frac{1}{1 + 2(1+\tau)\tan^2\theta_{e'}/2}, \qquad \varepsilon' = \sqrt{(1-\varepsilon^2)\tau(1+\tau)} \quad (3)$$

$$\varepsilon'' = \varepsilon'(1 - 4\sin^2\theta_W), \qquad \sigma_p = \varepsilon(G_E^{p,\gamma})^2 + \tau(G_M^{p,\gamma})^2 \quad (4)$$

With $\mathcal{K} = \frac{G_F Q^2}{\pi\alpha\sqrt{2}}$ and $\tau = Q^2/4M^2$.

If the radiative corrections are neglected, the expressions of the coefficients $\xi_V^p, \xi_V^n, \xi_V^{(0)}$ are given by Musolf et al. [?] as $\xi_V^p = 1 - 4\sin^2\theta_W$, $\xi_V^n = -1$, $\xi_V^{(0)} = -1$. The terms $G_E^{p,\gamma}$, $G_E^{n,\gamma}$, $G_M^{p,\gamma}$, $G_M^{n,\gamma}$ and $G_A^{T=1}$, $G_A^{T=0}$ are the electromagnetic Sachs form factors and G_E^s, G_M^s and G_A^s the weak Sachs form factors.

2 The PVA4 Experiment at MAMI

2.1 The experimental conditions

The experiment is performed at the MAMI facility at IKP Mainz University using the polarized electron beam close to the present maximum energy of 0.855 GeV. The square of the relative statistical uncertainty is proportional to the inverse of the Factor of Merit (FOM) defined as the product of the square of the asymmetry A by the differential cross section $d\sigma/d\Omega$. The elastic differential cross section is calculated using the electromagnetic form factors parameterized as usual [?]. The asymmetry, used in the FOM, is calculated without any strange form factors in the proton and without the electro-weak radiative corrections, with the recent PDG value $\sin^2\theta_W$=0.23117 [?]. The maximum is located around 35°± 5°. The value of the transfer momentum Q^2 at $\theta = 35°$ is equal to 0.227 (GeV/c)^2, while the value, weighted by the elastic cross section for 5 rings, taken into account the detector geometry and the target thickness, is $\langle Q^2 \rangle = 0.236 \pm 0.025$ (GeV/c)^2. At 35°, the value of A_0, the asymmetry without explicit strangeness, is expected to be equal to

-6.39 ppm under the preceding assumptions. The value of this asymmetry, weighted by the differential cross section over the angular range, is $< A_0 >= -6.78$ ppm. Using the parameters of Hammer [?] in a Dipole-Galster parameterization for the strange form factors, the predicted values of A_s (without radiative electro-weak corrections) are -9.44 ppm and $< A_s >= -9.99$ ppm respectively. For the central angle of 35°, this experiment measures a combination of electric and magnetic strange form factors given by: $G^s_E + 0.218 G^s_M$.

2.2 Experimental Setup

The experimental set up is shown in Fig. **??**. Polarized electrons with a polarization $|P_e|$ of about 80% are extracted from the strained AsGa source and accelerated in

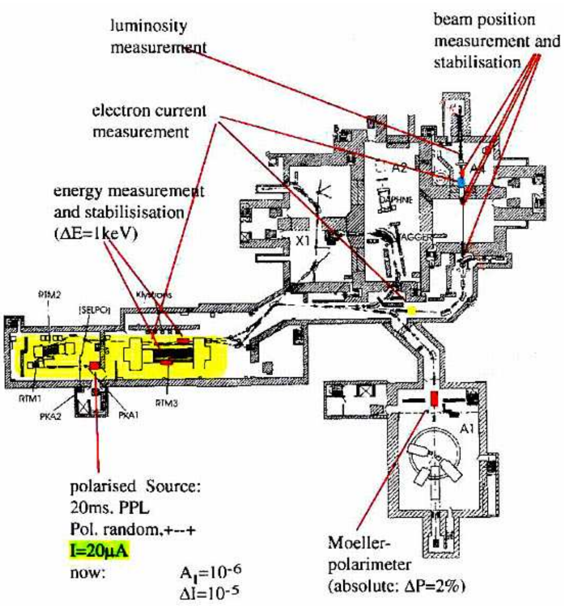

Fig. 1. Overview of the experimental setup

the MAinz MIcrotron in three stages to an energy of 0.8543 GeV. The 20 μA extracted electron beam is then focused on a liquid hydrogen target in the A4 hall. The necessary luminosity $\simeq 5.10^{37}\ cm^{-2}s^{-1}$ is achieved with a high cooling power, high flow liquid hydrogen target [?] of 10 cm length. At this intensity, the electron beam deposits 80 W of heating power in the target. The polarization of the beam is regularly measured with a Möller polarimeter by switching the beam in the hall A1. The electron current, energy, beam position and angle are continuously measured on beam line using a combination of resonant cavities. The energy of the particles scattered out of the target is absorbed in a PbF_2 Čerenkov shower calorimeter. The luminosity is measured at small angle after the target. The beam is then caught in a water cooled beam dump.

2.3 Polarized Electron Source and associated uncertainties

A laser is used to provide a linearly polarized light which is converted into a circular polarization using a $\lambda/2$ plate and a Pockels cell. Polarized electrons are produced by illuminating a strained GaAs photo-cathode with this laser light, the polarization of the light being transmitted to the electrons [?]. The helicity of the electrons is pseudo randomly reversed in 100 μs by switching the laser light polarization from right to left (or reverse). This is done by changing the sign of the applied high voltage to the Pockels cell. Each polarization state is maintained during a measurement gate time of nominally 20 ms in order to integrate out any fluctuation due to the European 50 Hz frequency. The time needed to reverse the polarization introduces a necessary random phase shift compared to the nominal frequency. The measurement gate lengths are continuously monitored for the two polarization states, and the false asymmetry introduced by this gate is measured, found lower than 10^{-9} and is therefore negligible. An intensity correlation at the electron source can induce an energy correlation. This energy correlation can propagate into a position and angle correlation of the electron beam on the target. It is therefore important to reduce the intensity correlation at the polarized source over the duration of the experiment. Therefore the angle of the $\lambda/2$ plate is adjusted during the measurements to obtain the same luminosity for each helicity state. The luminosity for each helicity state is measured continuously during the data acquisition. The absolute value of the polarization may be different in each helicity state. A second $\lambda/2$ plate may be introduced in the laser light before the Pockels cell to reverse the global sign of beam polarization and to allow the minimization of this difference. Half of measurements are done with this plate in, and half with the plate out. The introduction or removal of this second plate is performed regularly.

2.4 Calorimeter and electronics

The total angular range covered by this experiment goes from 30.14° to 44.19° taking into account the target size, where the FOM is maximum for the chosen energy ($\simeq$0.855 GeV). The counting rate, including elastic scattered electrons and background events, is very high ($\approx 10^8$/s). Therefore the calorimeter must be segmented and the material must be very carefully selected. The electronics has been especially developed for this experiment [?]. Systematic changes in the measured asymmetry due to pile-up as well as to dilution of elastic scattering events with inelastic processes nearest in energy have to be avoided. Therefore a very compact material with a fast response time ($<$ 20 ns) is needed which in addition can stand the high dose of ionizing radiation collected during the whole measurement time. Associated with the good energy resolution needed for the separation of elastic events, we found that Lead fluoride (PbF_2) single Čerenkov crystals is the best material and has been chosen [?]. The calorimeter is built of 1022 Čenrenkov crystals distributed in 7 rings of $\Delta\theta$=1.43°. Each crystal corresponds to $\Delta\phi$=2.47°. For the present experiment two sectors corresponding only to one half of the calorimeter have been built and 5 rings, corresponding to $31.4° < \theta < 42.4°$, used.

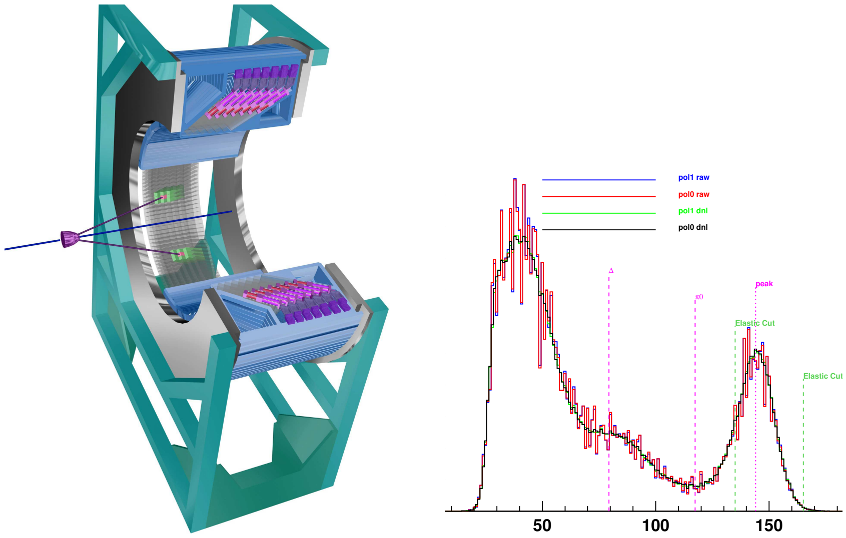

a) **b)**

Fig. 2. a):Schematic of the Čerenkov calorimeter b):Typical spectrum showing the elastic peak and the inelastic events. The shoulder is due to the Δ excitation.

A schematic view of the detector is shown in fig. **??** illustrating the principle of the detection. In order to obtain the needed energy resolution for the detected electrons, the collection of all the electromagnetic shower is needed. Therefore the sum of nine measured signals in a matrix of 3x3 crystals is done on line. The achieved energy resolution is about $4\%/\sqrt{E}$. A typical spectrum is displayed in fig. **??**. The signal of the Čerenkov calorimeter is substantially different from high energy electrons or photons and heavier charged particles where the Čerenkov photon yield is suppressed. The radiation damage can be healed completely by shining visible light on the material. Taking into account of the very high counting rate ($\simeq$100 kHz per crystal), a parallelization in the electronics and data acquisition system is needed to eliminate each kind of pile-up. Each cluster of 3x3 modules has individual, self triggering electronics. To avoid the spatial pile-up, we inhibit a second hit in neighborhood of the crystal hit in first. To eliminate the temporal pile-up, a second hit within the integration time is also inhibited. The signals coming from each cluster are summed up then integrated using analogical electronics. A total acquisition dead time of 20ns, including the pile-up rejection, has been obtained. After digitization, the localization in the calorimeter as well as the deposit energy in crystal are histogrammed.

3 Correction of the helicity correlated false asymmetry

3.1 Possible systematic uncertainties and their correction

The experimental asymmetry is defined for the present experiment by :

$$A_{exp} = \frac{\frac{N_e^+ I_e^+}{n^+} - \frac{N_e^- I_e^-}{n^-}}{\frac{N_e^+ I_e^+}{n^+} + \frac{N_e^- I_e^-}{n^-}} \tag{5}$$

$N_e^{\pm}$ being the detector counting rates in the two helicity states, $n^{\pm}$ the corresponding luminosity detector (described below) counting rates and $I_e^{\pm}$ the beam intensity in these helicity states. Under the assumptions of *(i)* a small background contribution to the elastic cross section, of *(ii)* an asymmetry associated to this background of the same order or weaker than the PV asymmetry, and *(iii)* a weak background contribution in the luminosity detectors, A_{exp} is given at the first order by :

$$A_{exp} = \frac{|P_e|\ A_{PV} + A_{I_e} + \delta^{RC}(1 + \frac{\mathcal{R}^b}{\mathcal{R}})A_{\mathcal{R}+\mathcal{R}^b}}{\delta^{RC}(1 + \frac{\mathcal{R}^b}{\mathcal{R}})} \tag{6}$$

where A_{PV} is the searched parity violation asymmetry. Its value, weighted by the differential cross section, is expected close to -6.78 ppm if we neglect the strangeness contribution and the electro-weak radiative corrections and use the PDG value for the weak mixing angle. Using the Musolf's estimations [?], the electro-weak corrections in our kinematic conditions are small and decrease the absolute value of A_{PV} of 7% ± 3%. The term A_{I_e} is the helicity correlated asymmetry in the incident intensity defined by $A_{I_e} = (I_e^+ - I_e^-)/(I_e^+ + I_e^-)$ where $I_e^{\pm}$ are the intensities of the electron beam in the two helicity states respectively. The term $A_{\mathcal{R}+\mathcal{R}^b}$ is the false asymmetry due to correlated fluctuations in energy, positions and angles of the electron beam. The δ^{RC} term is a correction to take into account the asymmetry in the electromagnetic radiative tail. In order to reduce the helicity correlated intensity fluctuations, the beam intensity is stabilized and the use of the second $\lambda/2$ plate allows, as previously indicated, to minimize the value of A_{I_e}. When the first $\lambda/2$ plate is introduced, the sign of the beam polarization $|P_e|$ as well as the helicity correlated false asymmetries are reversed but not the sign of the non helicity correlated false asymmetries. Therefore the difference between the values obtained for A_{exp} with and without this plate does no longer contain the non helicity correlated asymmetries. As an example, the target density fluctuations are not correlated to helicity and will disappear with this procedure. The luminosity measurement is continuously done using height integrating water Čerenkov counters regularly laid out on a cone and viewing the target at small scattering angle (4° to 10°) where the PV asymmetry is expected to be very weak [($\simeq$-4. ± 0.24) 10^{-8}]. The target density fluctuations (boiling, temperature effects,...) appear as a broadening in the distribution of the counting rates yielded in these luminosity monitors. The electron current is continuously measured at three positions in the beam line (see fig.**??**) and permits the calculation of A_{I_e} for each run ($\simeq$ 5 mn) as well as the pertaining corrections. Stabilization of the current is done using a feed back loop on the intensity monitors. In the present experiment we find $A_{I_e} = (7.5 \pm 23)\ 10^{-8}$. The false asymmetry $A_{\mathcal{R}+\mathcal{R}^b}$ contains the helicity correlated geometrical effects. We have :

$$A_{\mathcal{R}+\mathcal{R}^b} = \frac{(\mathcal{R}^+ + \mathcal{R}^{b+}) - (\mathcal{R}^- + \mathcal{R}^{b-})}{(\mathcal{R}^+ + \mathcal{R}^{b+}) + (\mathcal{R}^- + \mathcal{R}^{b-})} \tag{7}$$

With :

$$\mathcal{R}^\pm = \frac{\Sigma^\pm}{\Sigma_L^\pm + \Sigma_L^{b\pm}} \qquad \mathcal{R}^{b\pm} = \frac{\Sigma^{b\pm}}{\Sigma_L^\pm + \Sigma_L^{b\pm}} \tag{8}$$

Where :

$$\Sigma^\pm = \int_0^{l^\pm} \rho^\pm(z)dz \int_{\Omega^\pm(z)} \frac{d\sigma(E^\pm,\omega)}{d\omega}\, d\omega \qquad \Sigma^{b\pm} = \int_0^{l^\pm} \rho^\pm(z)dz \int_{\Omega^\pm(z)} \frac{d\sigma^b(E^\pm,\omega)}{d\omega}\, d\omega \tag{9}$$

and :

$$\Sigma_L^\pm = \int_0^{l^\pm} \rho^\pm(z)dz \int_{\omega_L^\pm(z)} \frac{d\sigma(E^\pm,\omega)}{d\omega}\, d\omega \qquad \Sigma_L^{b\pm} = \int_0^{l^\pm} \rho^\pm(z)dz \int_{\omega_L^\pm(z)} \frac{d\sigma^b(E^\pm,\omega)}{d\omega}\, d\omega \tag{10}$$

We also define:

$$\mathcal{R} = \frac{1}{2}(\mathcal{R}^+ + \mathcal{R}^-) \qquad \mathcal{R}^b = \frac{1}{2}(\mathcal{R}^{b+} + \mathcal{R}^{b-}) \tag{11}$$

$$\Sigma = \frac{1}{2}(\Sigma^+ + \Sigma^-) \qquad \Sigma^b = \frac{1}{2}(\Sigma^{b+} + \Sigma^{b-}) \tag{12}$$

$d\sigma(E^\pm,\omega)/d\omega$ and $d\sigma^b(E^\pm,\omega)/d\omega$ are the elastic and background cross sections respectively. $\Omega^\pm(z)$ and $\omega_L^\pm(z)$, which are the solid angles of the Čerenkov and of the luminosity detector seen from the point z in the target for the two helicity states, depend on the beam position (x,y) and angle $(\dot{x},\dot{y})$ which may be helicity correlated. The target thickness in the two helicity states $\ell^\pm$ are depending also on (x,y) and $(\dot{x},\dot{y})$. It can be shown that the effect of the target inhomogeneity is negligible in the case of the PVA4 experiment [**?**]. The target density $\rho^\pm(z)$ can be replaced by their mean values $< \rho^\pm >$. The advantage of the definition used for A_{exp} (Eq. **??**) is that the mean values $< \rho^\pm >$ itself disappears in the ratios of Eq. **??**. Moreover the eventual difference in the time of measurement in the two helicity states also disappears in that case. The distribution of the counting rate yielded by the luminosity monitors during a run gives some information on the ρ distribution. An increase of the width of such a distribution is an indication of a possible boiling of the target. The elastic cross section as well as the background cross section may be correlated to helicity via the beam energy $E^\pm$. Energy, beam positions and angles are continuously measured using a combination of resonant cavities on the beam line (See Fig. **??**). A feed back loop permits to stabilize these quantities using steering magnets on the beam line for the beam positions and angles. The width of the beam energy distribution is typically of 2 keV with the energy stabilization. The positions are stabilized within about 50 μm. During the experiment the helicity correlated positions and angles differences are $\delta x = 8 \pm 1$ nm, $\delta y = 82 \pm 2.9$ nm, $\delta\dot{x} = (1.7 \pm 0.18)10^{-7}\ ^\circ$, $\delta\dot{y} = (3.5 \pm 0.22)10^{-7}\ ^\circ$ and the helicity correlated energy difference is of about 5.2 ± 0.2 eV for the whole runs. As these differences are small, it may be possible to obtain an analytic estimation of $A_{\mathcal{R}+\mathcal{R}^b}$ neglecting the helicity correlations in $\Omega(z)$, $\omega_L(z)$ and ℓ . Using this approximation and neglecting the background, the asymmetry depends only on the elastic cross section. Using the typical experimental ΔE value of 5.2 ± 0.2 eV we find : $|A_{\mathcal{R}+\mathcal{R}^b}| \simeq 6.20 \pm\ 0.2\ 10^{-9}$. In the true experiment, the small values of the positions and angle fluctuations are taken into account using a linear χ^2 procedure. It has been shown [?] that partial compensations may occur between the corrections A_{I_e} and $A_{\mathcal{R}+\mathcal{R}^b}$ so these two terms are to be obtained together through the preceding χ^2 method. We then write:

$$A_{exp} = \frac{|P_e|\ A_{PV}}{\delta^{RC}(1 + \frac{\mathcal{R}^b}{\mathcal{R}})} + \sum_{i=1}^{6} a_i \Delta X_i \tag{13}$$

where : $\Delta X_i = X_i^+ - X_i^-$ and $X_i(i = 1, 6) = \{I_e,\ x,\ y,\ \dot{x},\ \dot{y}, E\ \}$ are the helicity correlated beam parameters. The a_i coefficients are experimentally obtained from the derivatives of the counting rates relative to the X_i parameters. This suppose a linear dependence of these counting rates versus the beam parameters.

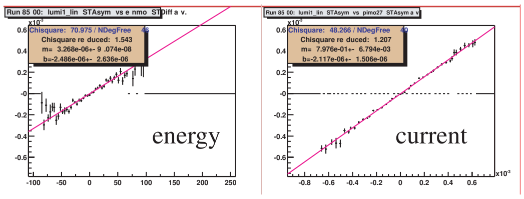

Fig. 3. Example of helicity correlated parameters

The linear dependence of the luminosity fluctuations on the beam parameters clearly appears in fig. ??. We give some preliminary results in the section ??. We notice that the false asymmetry term $A_{P_e} = (|P_e^+| - |P_e^-|)/(|P_e^+| + |P_e^-|)$ corresponding to the helicity correlated fluctuation in the value of the beam polarization does not contribute, at the first order, to the experimental asymmetry. The physical asymmetry is then given by:

$$A_{PV} = \frac{A_{exp} - \sum_i a_i \Delta X_i}{|P_e|}\ \delta^{RC}\left(1 + \frac{\mathcal{R}^b}{\mathcal{R}}\right) \tag{14}$$

The correction term $\delta^{RC}(1 + \mathcal{R}^b/\mathcal{R})$ contains δ^{RC} which takes into account the Q^2 dependence of the asymmetry in the radiative tail and a dilution factor which take into account of the presence of a physical background.

3.2 Extraction of the physical asymmetry

In figure **??**b) the typical spectrum shows a large elastic peak with some additional events above the pion threshold. Besides the contribution of the elastic radiative tail, some photons coming from high energy π^0 decay contribute to the small background under the elastic peak. Due to the intrinsic resolution of the detector, the inelastic electrons coming from the electroproduction of pions have to be considered. The associated cross sections have been calculated [**?**, **?**]. The magnitude of the background and radiative tail relative to the elastic peak depend on energy. We have to choose the lower energy cut to minimize the dilution effect and calculate the corresponding correction term. A Monte Carlo simulation [**?**], taking into account the cluster structure, was done to generate the shape of the experimental spectrum. For each Čerenkov crystal the correction term is then obtained as a function of the energy cut. This simulation includes the energy and angular straggling and the external radiative tails of the electrons as well for the incident beam as for the scattered electrons. The individual responses, experimentally measured [**?**], of each crystal are also included. In the fig. **??** the so obtained spectrum is compared with the experimental one.

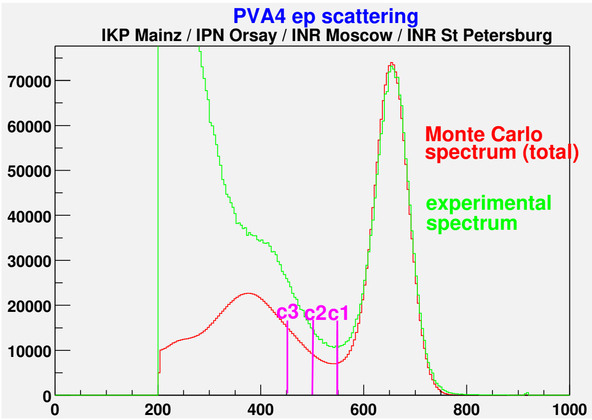

Fig. 4. Simulated and measured spectra versus the scattered electron energy in MeV.

Table 1. Correction term versus cuts in scattered electron energy

	$c3 = 0.45GeV$	$c2 = 0.50GeV$	$c1 = 0.55GeV$
$\mathcal{R}^b/\mathcal{R}$	9.7%	3.9%	1.68%
δ^{RC}	1.10	1.006	1.002
$\delta^{RC}\ (1+\mathcal{R}^b/\mathcal{R})$	1.108	1.045	1.019

The δ^{RC} term is obtained from the asymmetry in the radiative tail calculated in the peaking approximation. The correction term $\delta^{RC}(1+\mathcal{R}^b/\mathcal{R})$ equal to $\delta^{RC}(1+\Sigma^b/\Sigma)$ at the first order is given for three energy cut values: c1, c2, c3, in the table **??**.

4 Preliminary results

A first analysis of the data obtained at 0.8543 GeV, leads to the following preliminary value for the experimental PV asymmetry:

$$A_{PV} = -7.3 \pm 0.45 \pm 0.84 \text{ ppm}$$

This experimental value is compared with a few theoretical predictions for $< A_s >$. In this analysis the corrections to obtain the physical asymmetry have been partially done and are still in progress.

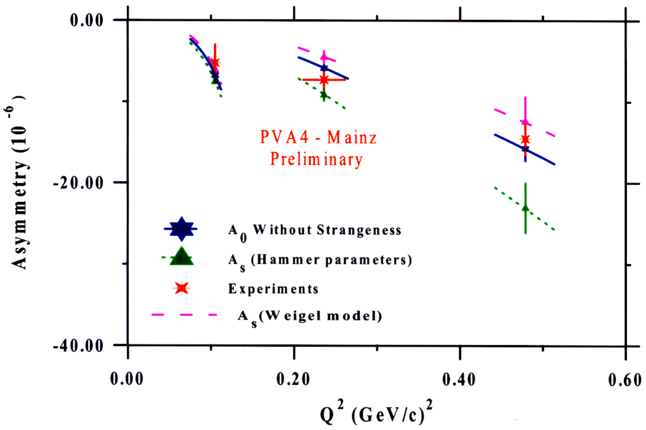

Fig. 5. Asymmetry: Measurements and predictions.

A more judicious choice of the limits taken for the elastic peak by using the corrections given in table **??** as well as the use of the data coming from the external rings of the calorimeter (which have been not presently included), will increase the statistical accuracy. The comparison with the results of the SAMPLE and HAPPEX experiments is done in fig.**??**. The theoretical predictions for $< A_0 >$ and $< A_s >$ are displayed for the three experiments, with the variation of the theoretical predictions in the measurement domains. In these predictions the electro-weak radiative corrections are not explicitly included but obtained with the effective values of $G_F = 1.1699\ 10^{-5}$, $\alpha = 1/135.144$ and $\sin^2(\theta_W) = 0.2388$ calculated by H. Spiesberger [**?**]. The asymmetry $< A_0 >$ has been calculated in the frame of the standard model assuming no strangeness in the weak form factors. The asymmetry $< A_s >$ includes the strange electric and magnetic form factors with the parameterization given by Hammer [**?**] or in the Weigel NJL model [**?**]. To evaluate the effect of these form factors, we can calculate their relative contribution defined as:

$$\delta_s^{th} = \frac{< A_s > - < A_0 >}{< A_0 >} \qquad \delta_s^{exp} = \frac{A_{PV} - < A_0 >}{< A_0 >}$$

These quantities are given for the three experiments and compared to the theoretical predictions of the Dipole-Galster parameterization with the Hammer parameters (a) and of the Weigel model (b) in the table **??**.

Table 2. Effect of the strangeness in PV experiments

Experiment	Q^2	δ_s^{exp}	δ_s^{th}
SAMPLE	0.105 ± 0.004	-0.298 ± 0.09	0.007 ± 0.03 (a) -0.175 ± 0.03 (b)
PVA4	0.236 ± 0.025	$0.239 \pm 0.08 \pm 0.14 \pm 0.07$	0.560 ± 0.1 (a) -0.235 ± 0.07 (b)
HAPPEX	0.477 ± 0.02	-0.109 ± 0.126	0.472 ± 0.07 (a) -0.206 ± 0.05 (b)

The three errors on δ_s^{exp} are coming respectively from the statistical error, the systematic uncertainty on A_{PV} and from the error on $< A_0 >$ due to the uncertainties on electromagnetic form factors and the uncertainty on beam energy. The systematic experimental uncertainty is coming from the errors in the false asymmetry correction terms (0.9% from A_{I_e}, 2% from the luminosity measurement, 0.3% from δx, 2.9% from δy, 0.1% from $\delta \dot{x}$, 0.3% from $\delta \dot{y}$ and 0.1% from δE.) The uncertainties on the theoretical predictions for PVA4 include the uncertainties on the electromagnetic form factors (giving 3.5% dominated by the uncertainty on the the neutron electric for factor which contribute for 2.9% then GEp for 1.39%, GMn for 1.26%, GA for 0.21% and GMp for 0.08%), and the uncertainty on beam energy coming from the multiple scattering in the target (1.7%). The value to be chosen for the weak mixing angle is a still open problem and may generates a large uncertainty which is not included in the preceding errors.

References

[1] P.E. Bosted, *Phys. Rev.* C **51**, 409 (1995), and references therein.
S. Galster et al., *Nucl. Phys.* B **32**, 221 (1971).

[2] D.E. Groom et al., *The European Pysical Journal* C **15**,1 (2000).

[3] H.W. Hammer et al., *Phys. Lett.* B **367**, 323 (1996).

[4] F.E.Maas and the A4 coll., Parity Violation in Atoms and Polarized Electron Scattering. *Word Scientific*, **491** (1999) Ed. by B. Frois and M.A. Bouchiat.

[5] K. Aulenbacher, C. Nachtigall et al., *NIM* A **391**, 498 (1997).

[6] P. Achenbach et al., *NIM* A **416**, 357 (1998).

[7] M.J. Musolf et al., *Phys. Rep.* **239**, 1 (1994).

[8] M. Morlet and J. Van de Wiele, *Report* **IPNO** (2002).

[9] S. Ong, M.P. Rekalo and J. Van de Wiele, *Eur. Phys. J.* A **6**, 215 (1999).

[10] J. Van de Wiele and S. Ong, *private communication.*

[11] B. Collin, *PhD Thesis* Orsay 2002

[12] F. E. Maas, Private communication.

[13] H. Spiesberger, Private communication.

[14] H. Weigel et al., *Phys. Lett.* B **353**, 20 (1995)